Electronic Supplementary Information for

Molecular Modulation of Nickel-Salophen Organic Frameworks Enables Selective Photoreduction of CO_2 at Varying Concentrations

Xiaohan Yu,‡[a,b] Mingzi Sun,‡[c] Tianran Yan,[a,b] Lin Jia,[a,b] Mingyu Chu,[a,b] Liang Zhang,[a,b] Wei Huang,*[a,b] Bolong Huang *[c,e] and Yanguang Li *[a,b,d]

[a] Institute of Functional Nano & Soft Materials (FUNSOM), Soochow University, Suzhou, 215123 China

[b] Jiangsu Key Laboratory for Advanced Negative Carbon Technologies, Soochow University, Suzhou 215123, China

[c] Department of Applied Biology and Chemical Technology, The Hong Kong Polytechnic University, Hung Hom, Kowloon, Hong Kong SAR 999077, China

[d] Macao Institute of Materials Science and Engineering (MIMSE), MUST-SUDA Joint Research Center for Advanced Functional Materials, Macau University of Science and Technology, Taipa 999078, Macau SAR, China

[e]Research Centre for Carbon-Strategic Catalysis, The Hong Kong Polytechnic University, Hung Hom, Kowloon, Hong Kong SAR 999077, China.

‡These two authors contribute equally.

E-mail: yanguang@suda.edu.cn; bhuang@polyu.edu.hk; weihuang@suda.edu.cn

Materials

All the chemicals and solvents were purchased from commercial sources and used as received unless otherwise noted.

Characterizations

SEM images were taken on a Supera 55 scanning electron microscope (Carl Zeiss AG, Oberkochem, Germany). TEM and EDS measurements were carried on an FEI Talos transmission electron microscope equipped with a Super-X EDS detector and operated at an accelerating voltage of 200 kV. Atomic-resolution HAADF-STEM images were recorded using a Thermo Fisher Themis Z microscope equipped with two aberration correctors at an operation voltage of 300 kV. PXRD was performed on a PANalytical X-ray diffractometer with monochromatic Cu Kα radiation. FT-IR spectra were recorded using a Bruker Vertex 70 FTIR spectrometer under the attenuated total reflection (ATR) mode. UV-Vis diffuse reflectance spectra were collected on a Perkin Elmer Lambda 950 spectrophotometer. Single-crystal XRD was carried out on a Bruker D8 Venture X-ray diffractometer at 298 K with a graphite-monochromated Cu Kα radiation source (λ = 1.54184 Å). The structure was solved with the ShelXS structure solution program, and refined with the XL refinement package using least squares minimization. The X-ray absorption spectra (XAS) were performed at the Shanghai Synchrotron Radiation Facility (SSRF) on the bending-magnet beamline 11B with an electron energy of 3.5 GeV and an average current of 200 mA. The radiation was monochromatized by a Si (111) double-crystal monochromator. N_2 sorption experiments were carried out using a Micrometrics ASAP 2020 HD88 analyzer. Samples were degassed at 120 °C under vacuum for 12 h prior to analysis. Liquid NMR spectra for all compounds were measured using a 400 MHz Bruker Avance NMR spectrometer. Steady-state fluorescence spectra were recorded on a Horiba FL3-211 spectrofluorometer under an excitation wavelength of 380 nm at room temperature. Time-resolved PL lifetime measurements were conducted with a FluoroHub single

photon counting controller. EPR data were recorded on a Bruker A300 EPR spectrometer under irradiation with a xenon lamp. CO_2 TPD measurements were performed on a FINESORB-3010 chemisorption analyzer. Samples were first degassed at 200 ℃ under vacuum for 1 h. CO_2 was then introduced for 30 min to achieve the adsorption equilibrium. Subsequently, samples were flushed with Ar for 30 min to remove atmospheric CO_2, and heated to 200 ℃ at a rate of 10 ℃ min^{-1} under a continuous Ar flow. Desorbed CO_2 was analyzed by a thermal conductivity detector (TCD).

Material synthesis

Synthesis of 1,3,5-tris(4-aminophenyl)triazine (TAPT):

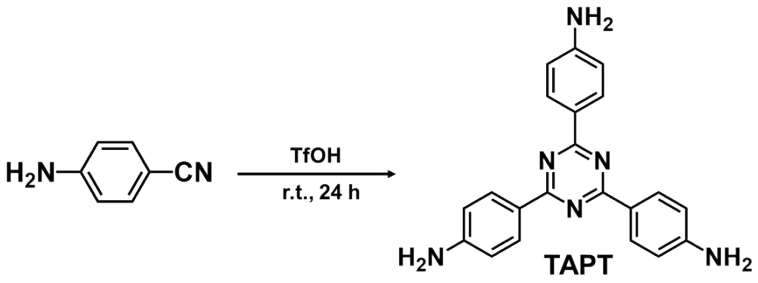

Trifluoromethanesulfonic acid (4.5 mL) was dropwise added into a 50 mL flask charged with 4-aminobenzonitrile (1.5 g, 12.7 mmol) at 0 ℃ under N_2. The mixture was stirred until the monomer was completely dissolved. The solution was then warmed to room temperature and stirred for 24 h. After the reaction, the mixture was diluted with 40 mL of H_2O under vigorous stirring and neutralized by aqueous ammonia until pH = 10. The precipitate was collected by centrifugation, washed with H_2O and ethanol, and finally dried at 80 ℃ under vacuum. ^1H NMR (DMSO-d_6, 400 MHz) δ (ppm) = 8.34 (d, 2 H), 6.70 (d, 1 H), 5.92 (s, 1H); ^{13}C NMR (DMSO-d_6, 400 MHz) δ (ppm) = 170.0, 153.4, 130.6 123.4, 113.6.

Synthesis of Ni-SOF

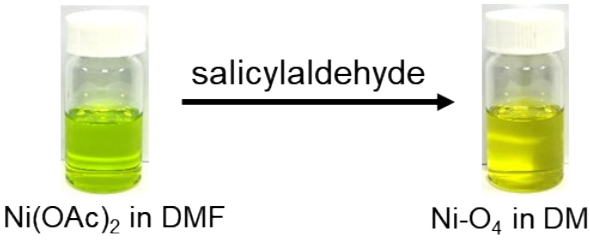

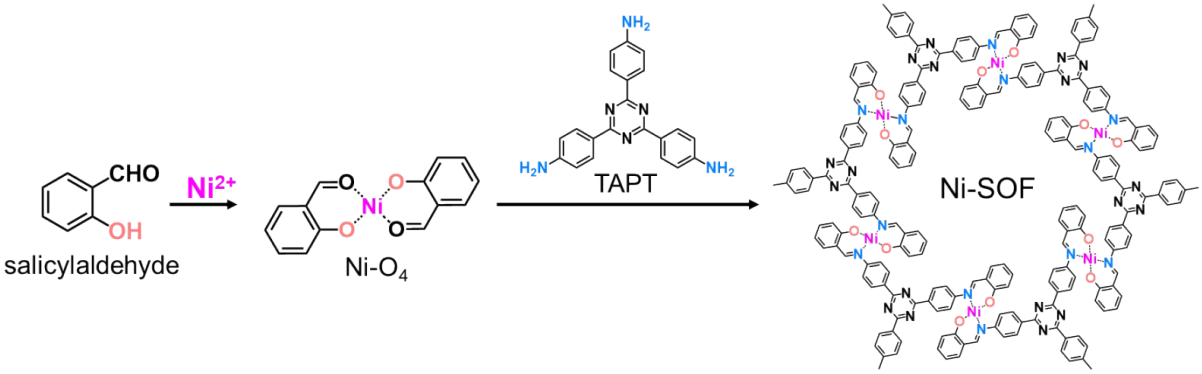

$Ni(OAc)_2 \cdot 4H_2O$ (224 mg, 0.9 mmol) and salicylaldehyde (188 μL, 1.8 mmol) were dissolved in 20 mL of DMF to form the soluble Ni-O_4 complex. After stirring for 30 min under N_2, TAPT (212.4 mg, 0.6 mmol) was added into the solution. The mixture was further stirred at 100 °C for 24 h under N_2. After cooling down to room temperature, the precipitate was collected by centrifugation, thoroughly washed with DMF, EtOH, and H_2O, and freeze-dried, giving rise to the titled sample as a yellow powder. The synthetic procedures for Co-SOF, Cu-SOF, and Zn-SOF were similar except that corresponding metal salts were added instead of $Ni(OAc)_2 \cdot 4H_2O$.

Synthesis of Ni-N_4 or Ni-N_2S_2

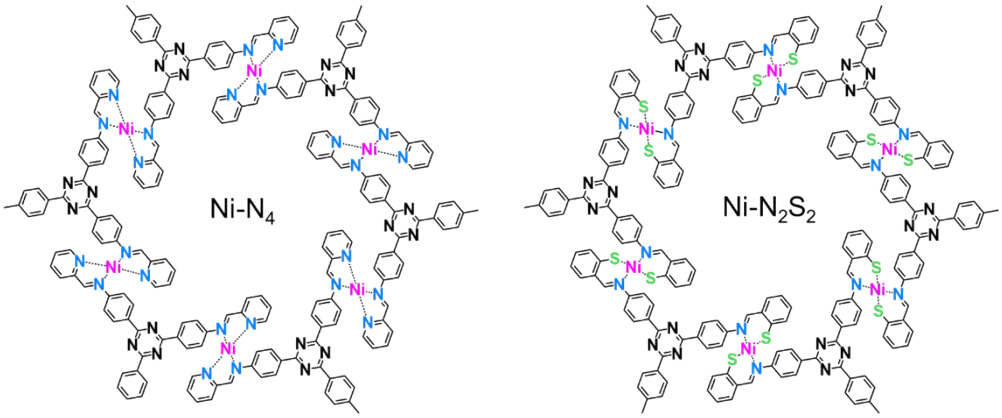

The synthetic procedures for Ni-N_4 or Ni-N_2S_2 were similar to that of Ni-SOF except that salicylaldehyde was replaced by 2-pyridinecarboxaldehyde and 2-mercaptobenzaldehyde, respectively.

Synthesis of Ni-salophen

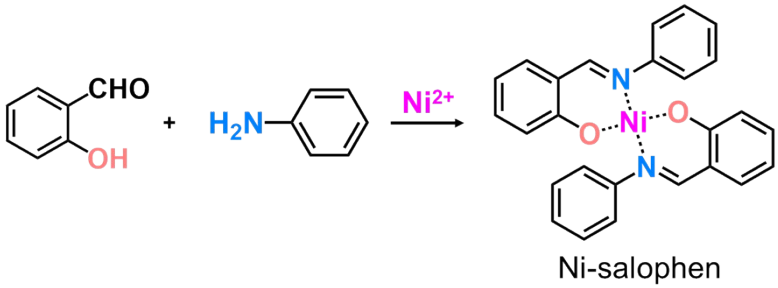

Ni-salophen was synthesized according to the literature with modification.[S1] In brief, $Ni(OAc)_2 \cdot 4H_2O$ (1.24 g, 5 mmol) and salicylaldehyde (1 mL, 10 mmol) were dissolved in 15 mL of methanol and refluxed at 70 °C for 1 h. A solution of aniline (0.91 mL, 10 mmol) in 5 mL MeOH was then dropwise added. The reaction solution was refluxed for another 2 h under N_2. After cooling down to room temperature, the formed precipitate was collected by filtration and washed with MeOH to yield the titled sample as a dark green solid. ^{1}H NMR ($CDCl_3$, 400 MHz) δ (ppm) = 6.97 (t, 2 H), 7.04 (d, 4 H), 7.30-7.42 (m, 10H), 7.46 (m, 2H), 8.66 (s, 2H). Single-crystal Ni-salophen for structural determination was prepared by the slow diffusion of MeOH into a saturated dichloromethane solution of Ni-salophen.

Photocatalytic measurements

Typically, 1 mg of catalyst and 12 mg of $[Ru(bpy)_3]Cl_2 \cdot 6H_2O$ were ultrasonically dispersed in a mixture of acetonitrile, H_2O, and TIPA (6:2:1, v:v:v, 9 ml) in a gas-tight quartz reactor. The reactor was bubbled with pure CO_2 or mixed CO_2/Ar gases (v/v = 20/80, 15/85, 10/90 or 5/95) for 30 min, and it was then irradiated by a 300 W Xe lamp (China Education Au-light, CEL-HXF300) equipped with a 420 nm cutoff filter. The reaction temperature was kept at 25 ℃ by a water circulation system. Evolved gaseous products were analyzed and quantified using a gas chromatograph (SHIMADZU 2010) equipped with a TCD and a flame ionization detector (FID) using Ar as the carrier gas. All photocatalytic reactions were repeated three times to ensure the accuracy of experimental data.

Apparent quantum efficiency (AQE) calculations

For the AQE measurements, Ni-SOF (1 mg) was dispersed in a mixed solution of MeCN/H_2O/TIPA (6:2:1, 9 mL). A 300 W Xe-lamp with a bandpass filter (λ = 420 nm, 450 nm, or 500 nm) was used as the light source. Its intensity was calibrated using an optical power detector (Newport, Model 1918-R) and adjusted to 12 mW cm^{-2}. The irradiation area was controlled to be 0.785 cm^2. The CO production was determined after 1 h irradiation. The AQE for CO production was estimated according to the following equation:

$$\mathrm{AQE} = 2 \times \frac{n\text{umber of produced CO molecules}}{n\text{umber of incident photons}} \times 100\%$$

$$= 2 \times \frac{Nco \times NA \times h \times c}{I \times S \times t} \times 100\%$$

where $\boldsymbol{N}co$ is the amount of produced CO (mol), N_A is the Avogadro constant (6.022×10^{23} mol^{-1}), h is the Planck constant (6.626×10^{-34} J·s), c is the speed of light (3×10^8 m s^{-1}), S is the

irradiation area (cm^2), I is the light intensity (W cm^{-2}), t is the photoreaction time (s) and λ is the wavelength of the monochromatic light (m).

Isotope labelling experiment

Isotopic experiment was conducted using $^{13}CO_2$ instead of $^{12}CO_2$ under otherwise identical conditions. Specifically, Ni-SOF (1 mg) was dispersed in a mixed solution of MeCN/H_2O/TIPA (6:2:1, 9 mL). The sealed reactor was vacuumed and charged with pure $^{13}CO_2$ and was then irradiated for 1 h using a 300 W Xe lamp. Gas products were analyzed by gas chromatography-mass spectrometry (GC-MS, 7890B-5977 A, Agilent, USA).

***Operando* DRIFTS**

Operando DRIFTS measurements were performed on a Thermo Fisher IS50 spectrometer. In brief, Ni-SOF (0.5 mg), $[Ru(bpy)_3]Cl_2 \cdot 6H_2O$ (1.2 mg), and TIPA (0.1 mL) were dispersed in a mixed solution of MeCN and H_2O (1 ml, v:v = 3:1) within a custom-built chamber. The solution was first purged with Ar for 1 h before bubbling with CO_2 for 30 min to achieve the absorption equilibrium. The background signal was first recorded in the dark. The sample was then irradiated under visible light (λ> 420 nm), and its DRIFTS signals were collected at specific time intervals. The resolution of the signals was set at 4 cm^{-1}.

Theoretical calculations

DFT calculations were performed through the CASTEP packages.[S2] In this work, we selected the generalized gradient approximation (GGA) and Perdew-Burke-Ernzerhof (PBE) as the main functionals to supply accurate descriptions of the exchange-correlation interactions.[S3-5] The plane-wave basis cutoff energy was set to be 380 eV based on the ultrafine quality and the ultrasoft pseudopotentials. For energy minimizations, the Broyden-Fletcher-Goldfarb-Shannon (BFGS) algorithm was considered with a coarse quality of k-point settings after convergence

tests.[S6] The separation of k-point was 0.7 $Å^{-1}$. Strict convergence criteria were adopted in this work for the geometry optimization. For Hellmann-Feynman forces, the relaxation should lead to a result smaller than 1×10^{-3} eV/Å. For energy calculations, the total energy difference should be converged to a value smaller than 5×10^{-5} eV/atom.

References

S1 J. W. Zhao, L. P. Song, Y. K. Wang, S. Z. Zhu, *J. Fluor. Chem.* 2006, **127**, 405-408.

S2 S. J. Clark, M. D. Segall, C. J. Pickard, P. J. Hasnip, M. J. Probert, K. Refson, M. C. Payne, *Z. Kristallogr* 2005, **220**, 567-570.

S3 J. P. Perdew, K. Burke, M. Ernzerhof, *Phys. Rev. Lett.* 1997, **78**, 1396.

S4 P. J. Hasnip, C. J. Pickard, *Comput. Phys. Commun.* 2006, **174**, 24-29.

S5 J. P. Perdew, J. A. Chevary, S. H. Vosko, K. A. Jackson, M. R. Pederson, D. J. Singh, C. Fiolhais, *Phys. Rev. B* 1992, **46**, 6671-6687.

S6 J. D. Head, M. C. Zerner, *Chem. Phys. Lett.* 1985, **122**, 264-270.

S7 R. N. Sampaio, D. C. Grills, D. E. Polyansky, D. J. Szalda, E. Fujita, *J. Am. Chem. Soc.* **2020**, 142, 2413-2428

S8 Z. Liu, J. Li, Z. Chen, M. Li, L. Wang, S. Wu, J. Zhang, *Appl. Catal. B Environ.* **2023**, 326, 122338

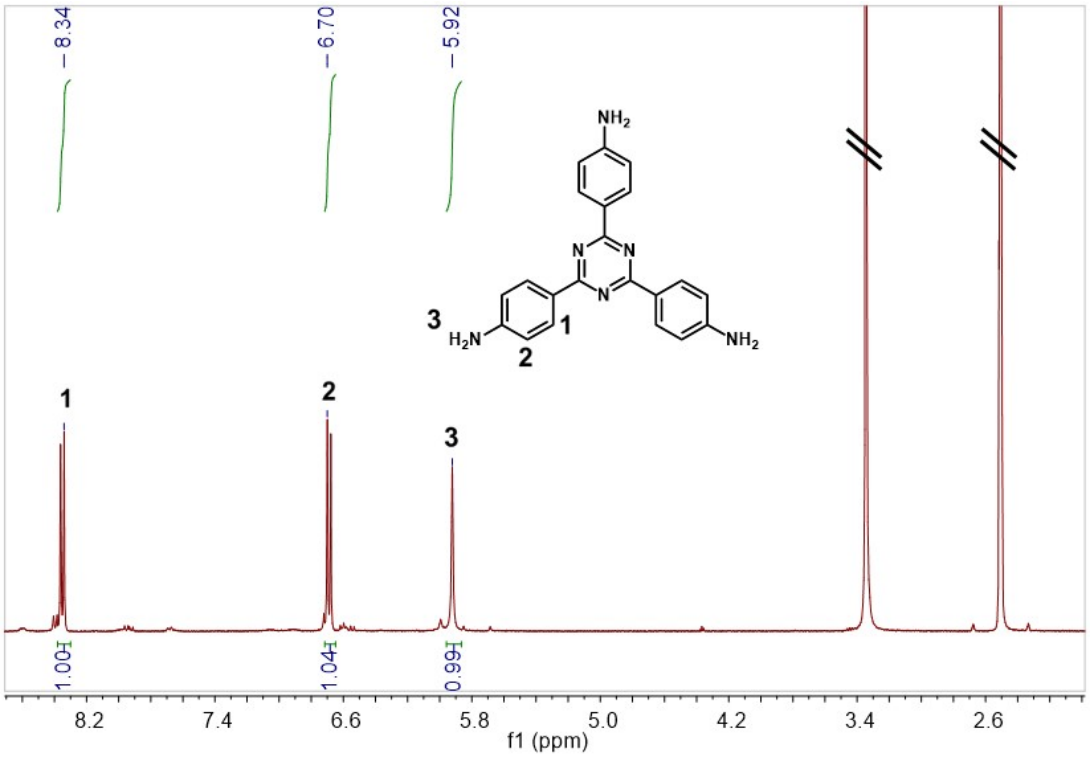

^{1}H NMR spectrum of TAPT (400 MHz, DMSO-d_6, at 298 K).

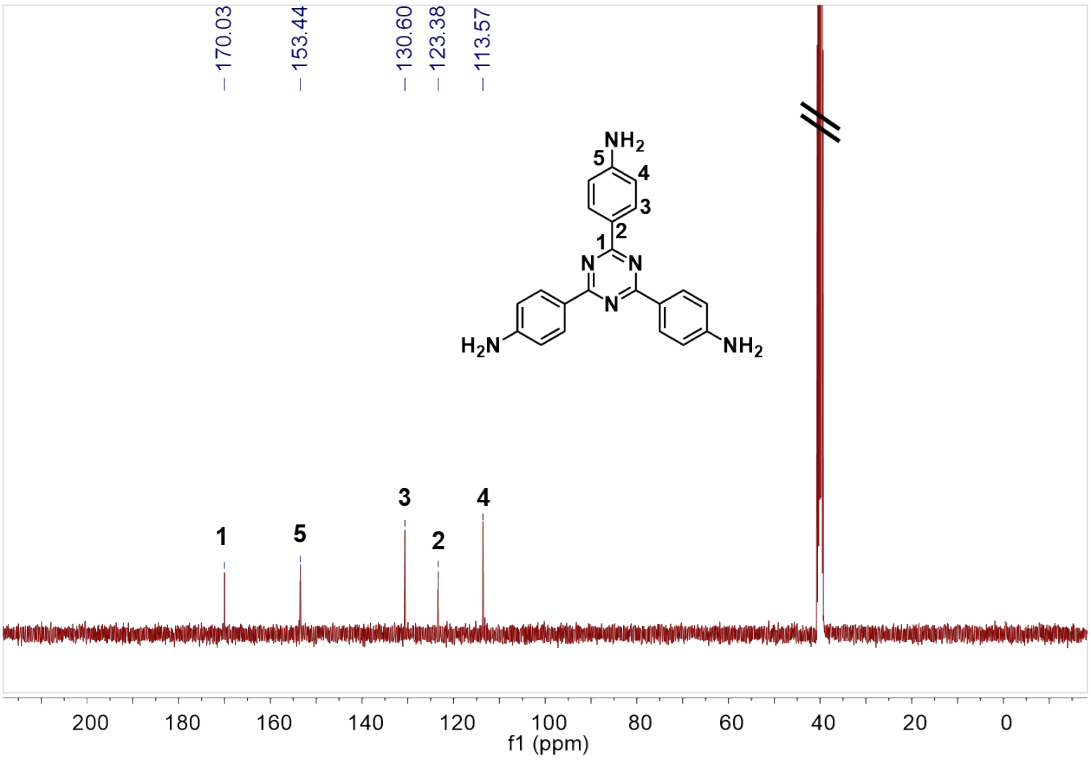

^{13}C NMR spectrum of TAPT (400 MHz, DMSO-d_6, at 298 K).

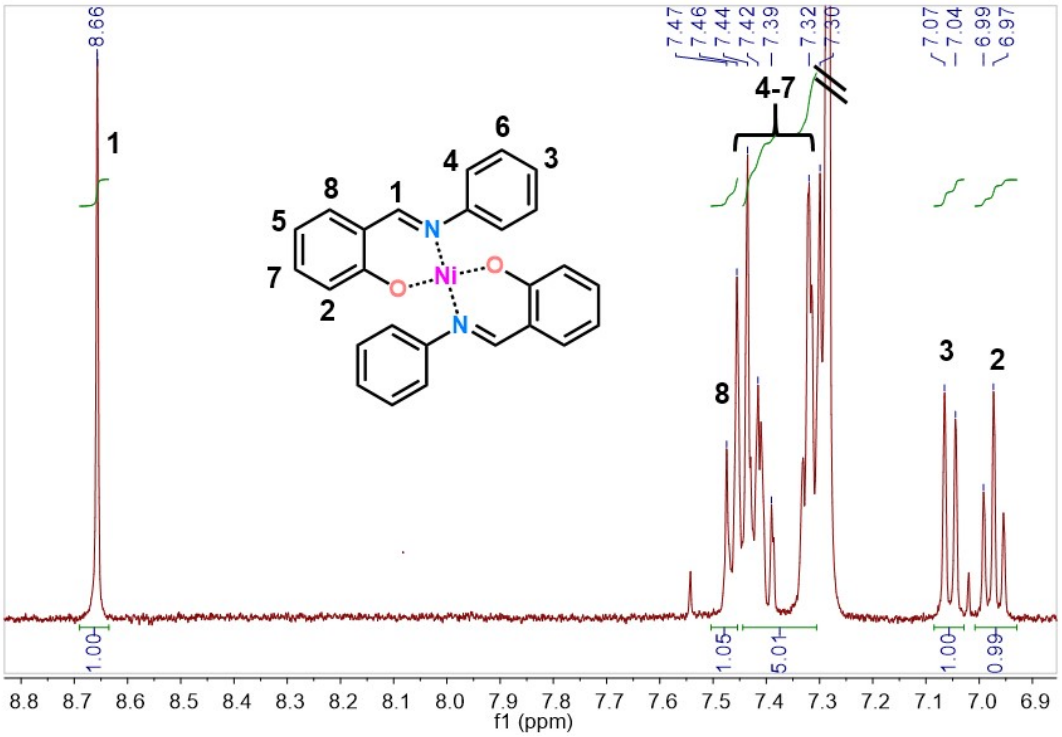

^{1}H NMR spectrum of Ni-salophen (400 MHz, $CDCl_3$, at 298 K).

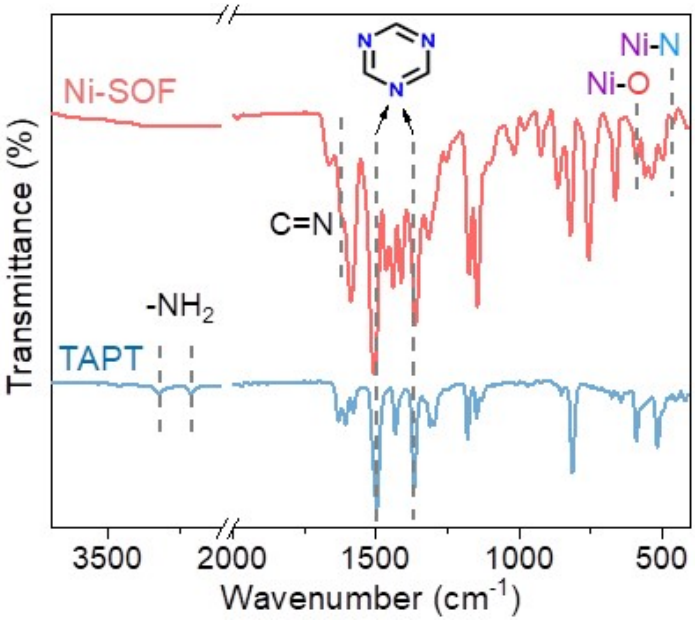

Fig. S1 FT-IR spectra of Ni-SOF and TAPT.

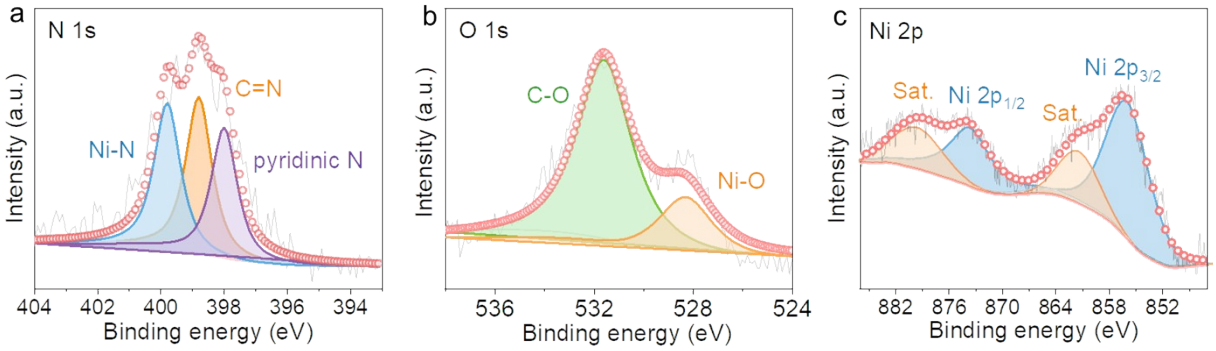

Fig. S2 (a) N1s, (b) O 1s, and (c) Ni 2p XPS spectra of Ni-SOF.

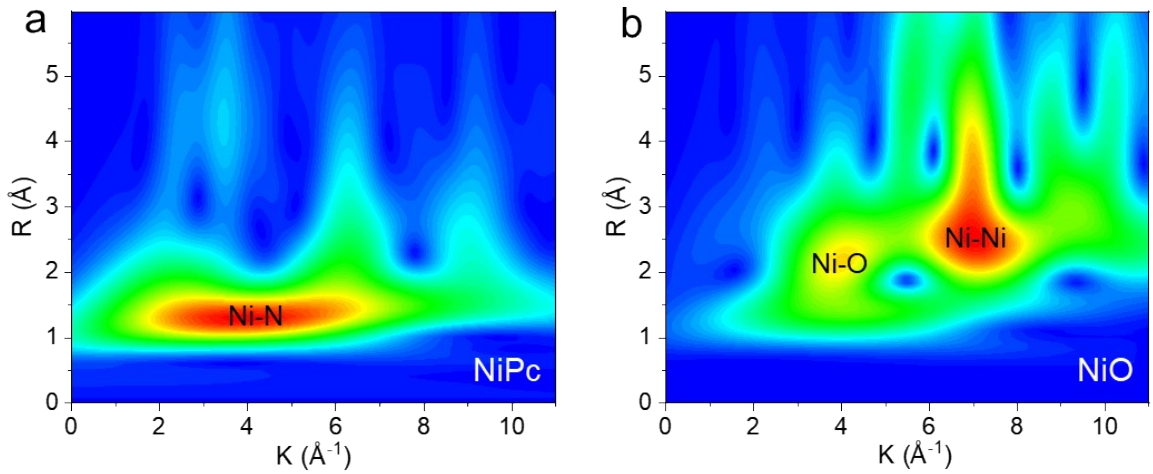

Fig. S3 Wavelet transform of the EXAFS spectra of (a) NiPc and (b) NiO.

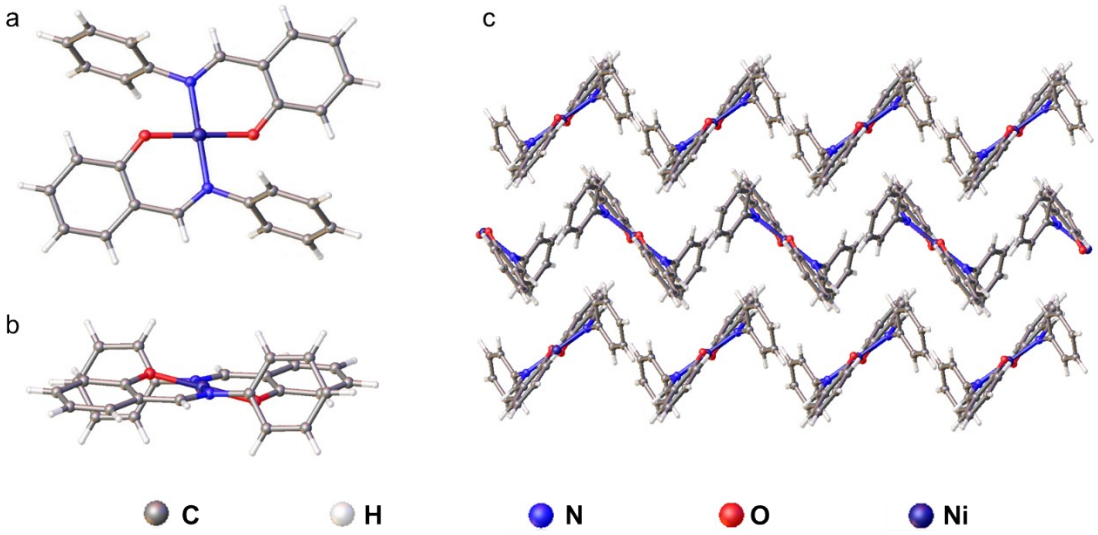

Fig. S4 (a) Top view, (b) side view, and (c) intermolecular arrangement of Ni-salophen derived from its single crystal XRD.

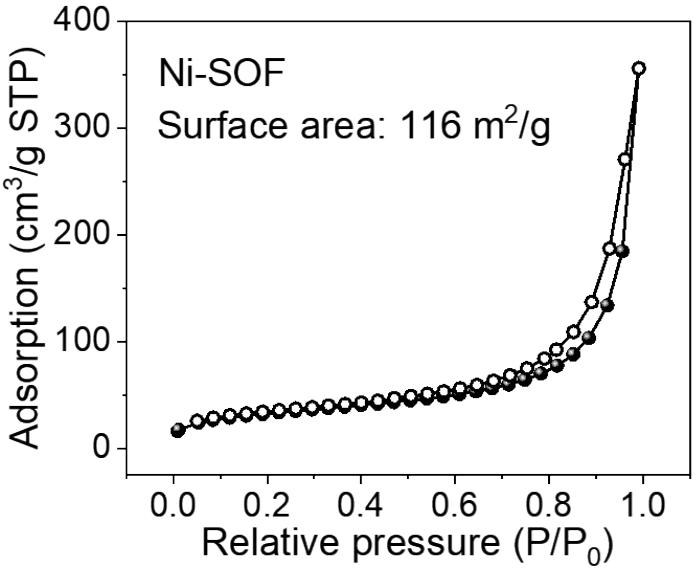

Fig. S5 Nitrogen sorption isotherm curve of Ni-SOF.

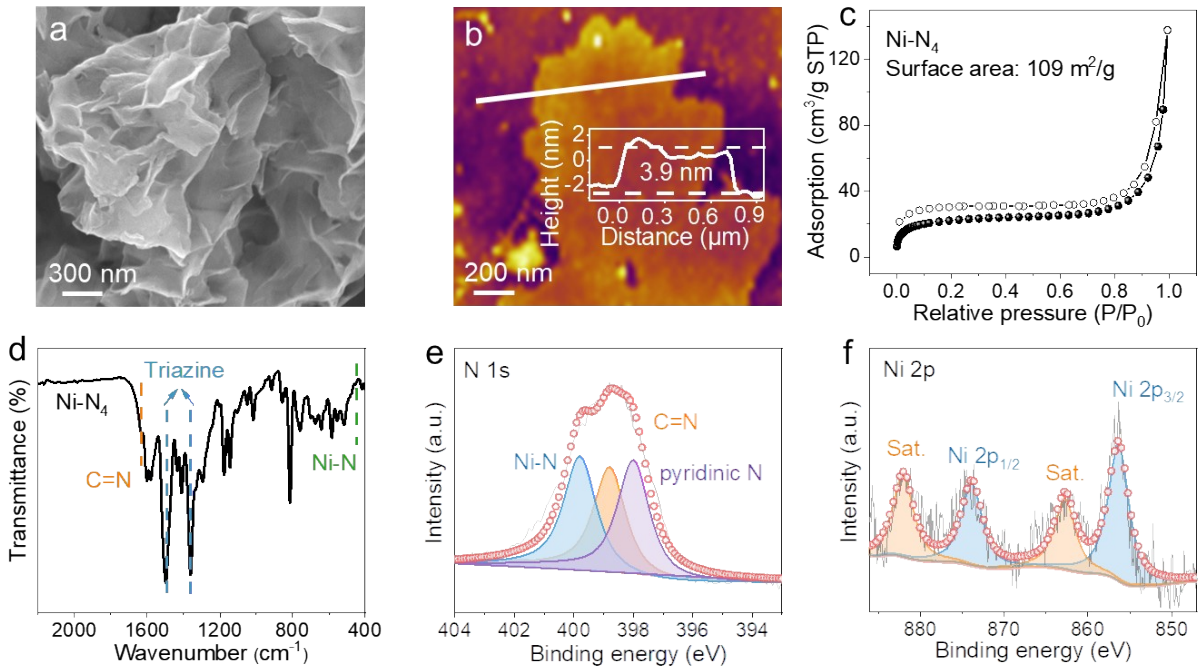

Fig. S6 (a) SEM image, (b) AFM image, (c) nitrogen sorption isotherm curve, (d) FT-IR spectrum, (e) N 1s XPS spectrum, and (f) Ni 2p XPS spectrum of Ni-N_4.

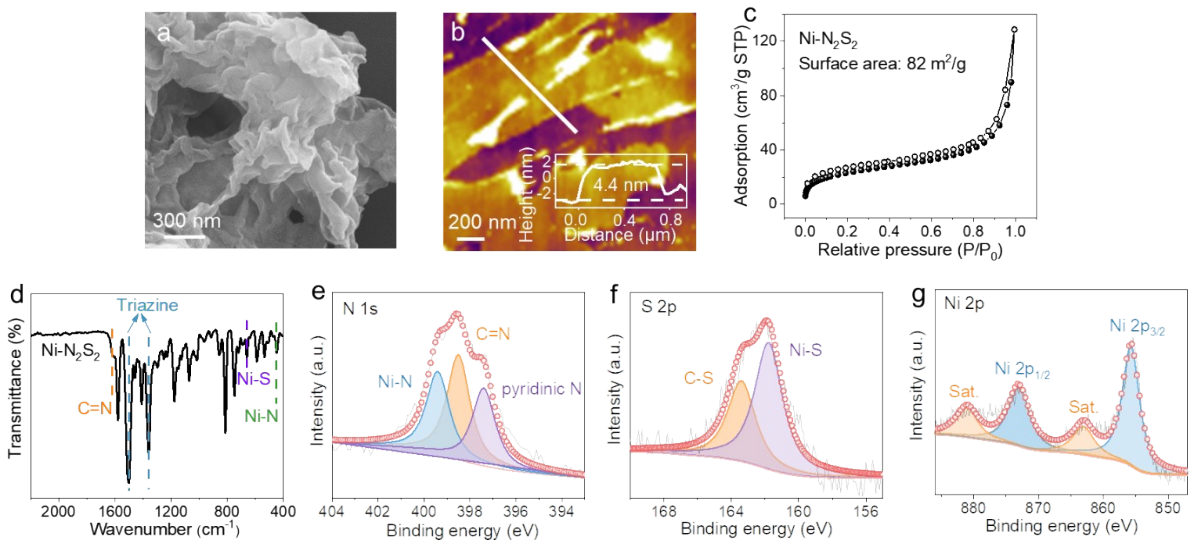

Fig. S7 (a) SEM image, (b) AFM image, (c) nitrogen sorption isotherm curve, (d) FT-IR spectrum, (e) N 1s XPS spectrum, (f) S 2p XPS spectrum and (g) Ni 2p XPS spectrum of Ni-N_2S_2.

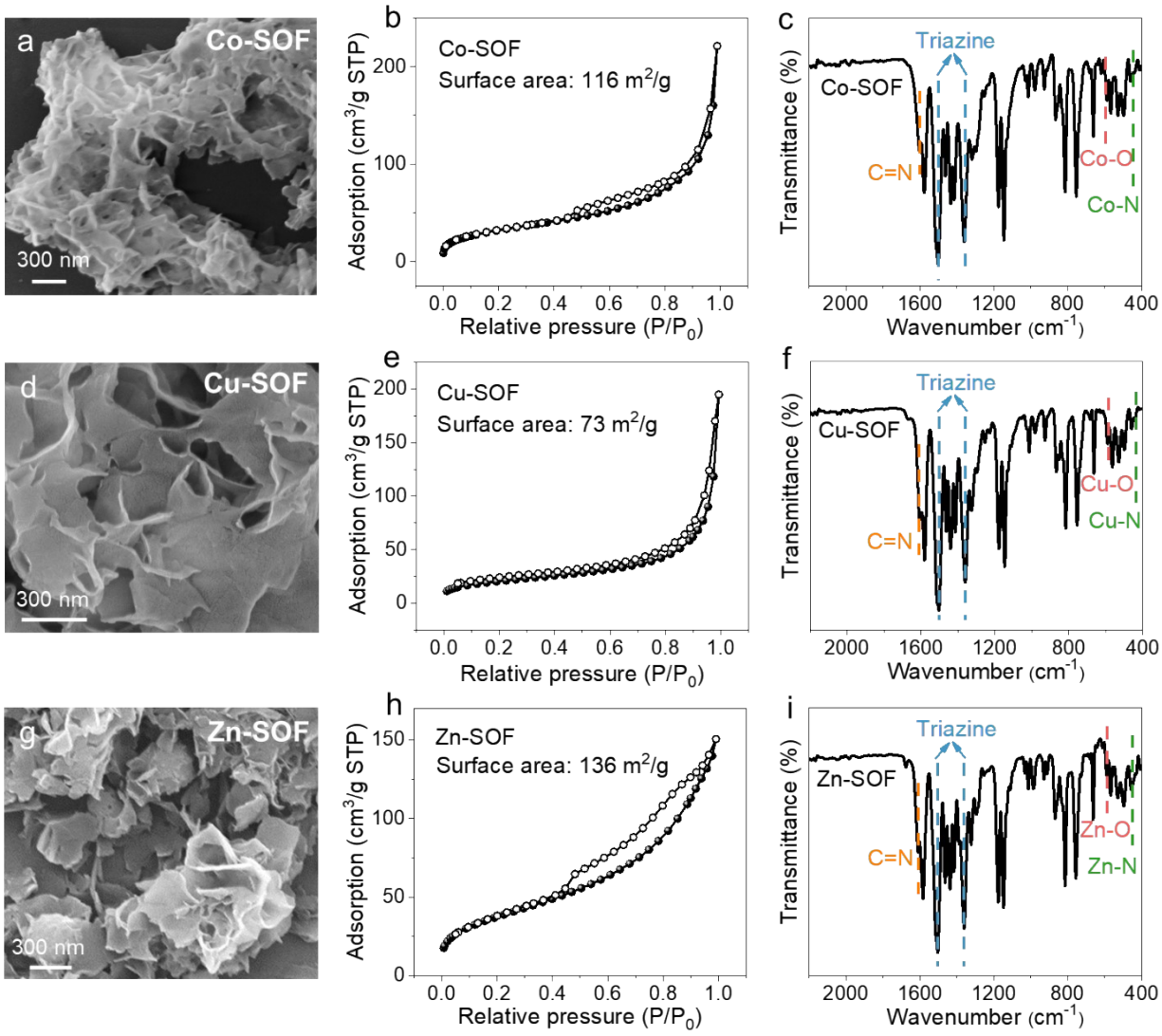

Fig. S8 (a) SEM image, (b) nitrogen sorption isotherm curve, and (c) FT-IR spectrum of Co-SOF. (d) SEM image, (e) nitrogen sorption isotherm curve, and (f) FT-IR spectrum of Cu-SOF. (g) SEM image, (h) nitrogen sorption isotherm curve, and (i) FT-IR spectrum of Zn-SOF.

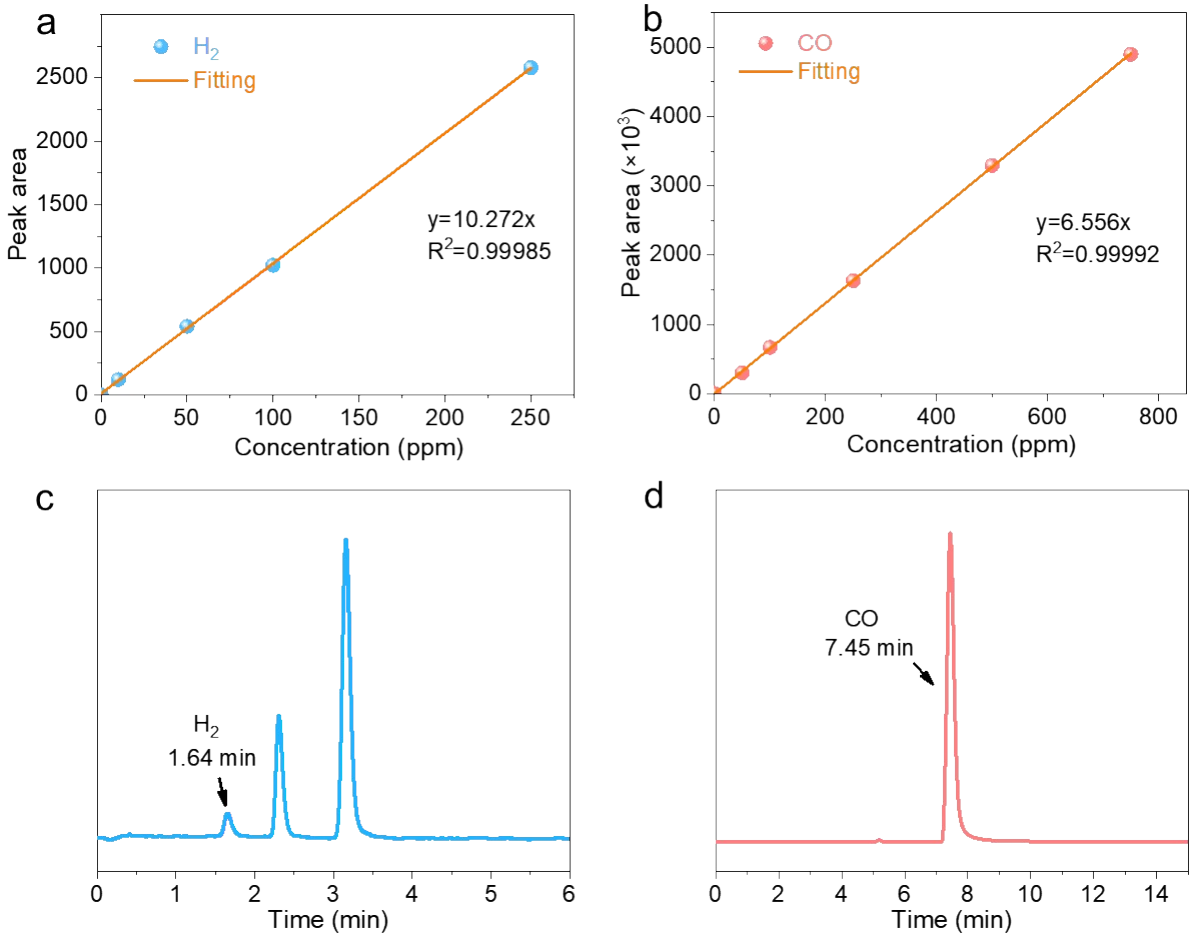

Fig. S9 (a,b) GC calibration curves of (a) H_2 and (b) CO. (c,d) Corresponding retention time of (c) H_2 and (d) CO.

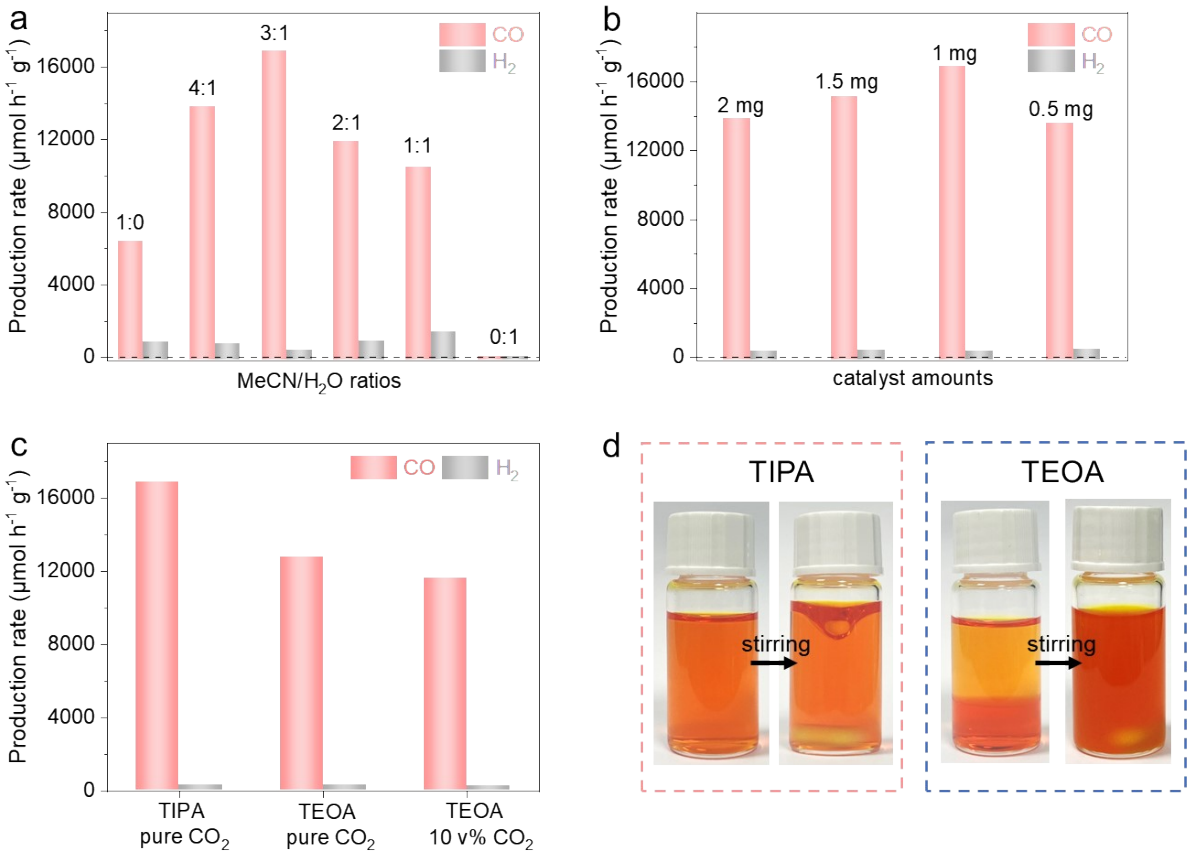

Fig. S10 (a-c) CO and H_2 production rates on Ni-SOF at different (a) MeCN/H_2O ratios, (b) catalyst amounts, and (c) hole scavengers. (d) Photographs of the reaction solution using TIPA or TEOA as the hole scavenger under static or stirring conditions.

Note: TEOA and TIPA were explored as the hole scavengers in our photocatalytic system. Compared to the photocatalytic performance achieved with TIPA, the activity drops to 76% of the value in the presence of TEOA under pure CO_2. The reduced activity in the presence of TEOA is likely caused by the phase separation of the MeCN/H_2O/TEOA mixture due to the formation of zwitterionic alkycarbonate structures [S7-S8]. As a result, TEOA and $Ru(bpy)_3Cl_2$ are partitioned into the water and organic layers, respectively. On the one hand, the phase separation of the reaction mixture would result in inadequate mixing and inefficient charge transfer between $Ru(bpy)_3Cl_2$ and TEOA. On the other hand, the formed turbid emulsion under stirring would significantly limit light penetration and reduce photon utilization efficiency. All

these factors collectively lead to compromised photocatalytic performance when using TEOA as the hole scavenger. By contrast, the use of TIPA as the hole scavenger maintains a monophasic reaction solution.

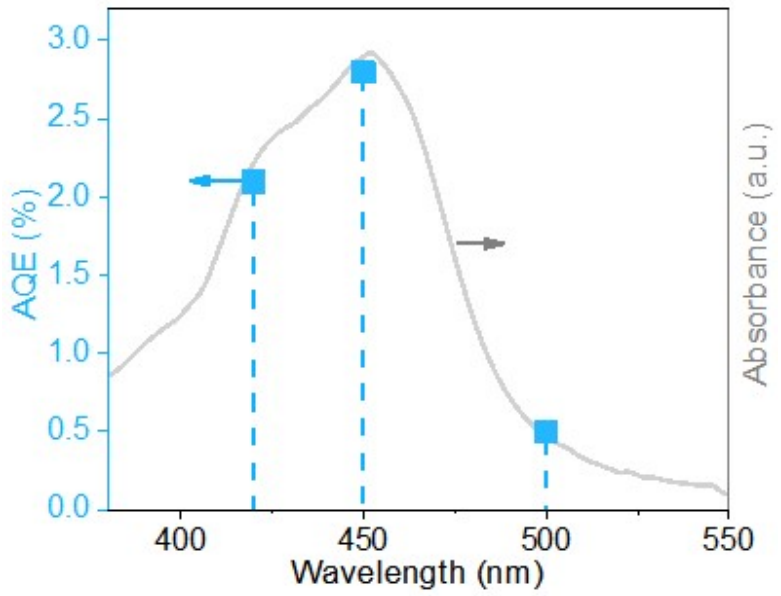

Fig. S11 AQE values of Ni-SOF at several selected wavelengths under pure CO_2 overlapped with the absorption spectrum of $Ru(bpy)_3Cl_2$.

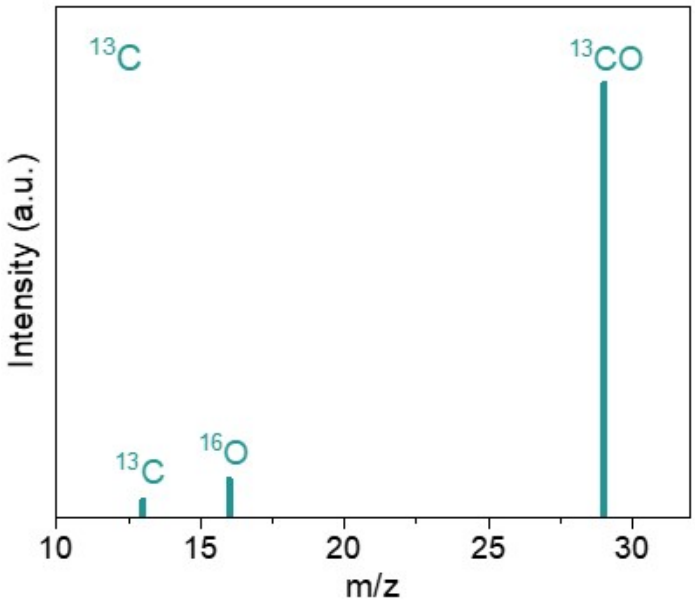

Fig. S12 GC-MS spectrum of generated CO from the photoreduction of $^{13}CO_2$.

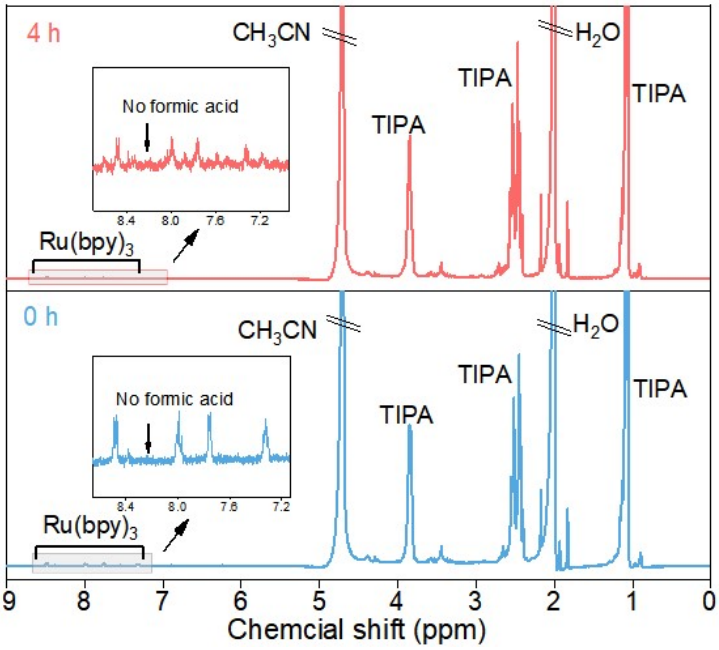

Fig. S13 ^{1}H NMR spectra of the typical photocatalytic reaction solution before and after 4 h irradiation.

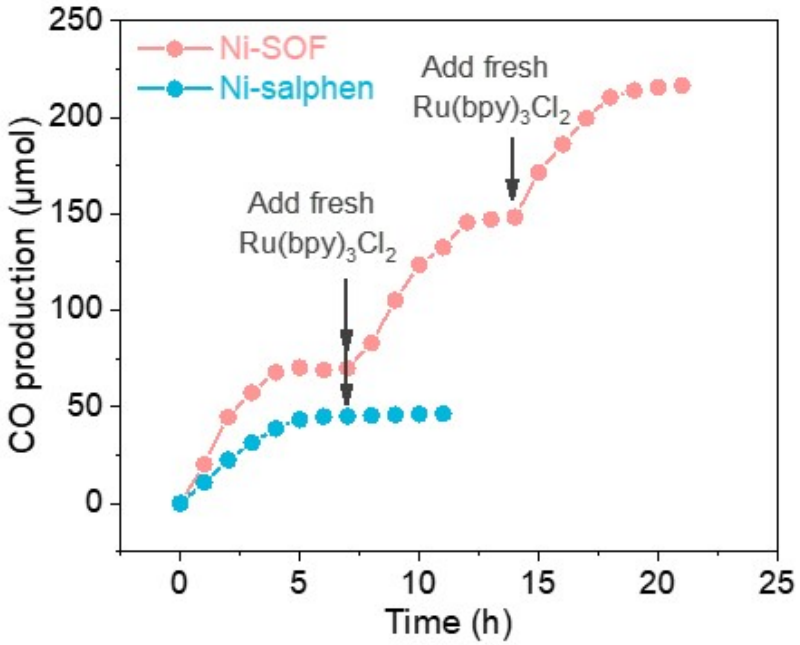

Fig. S14 Photocatalytic performances of Ni-SOF and Ni-salophen after the addition of fresh $[Ru(bpy)_3]Cl_2$ (12 mg) as indicated by the arrows.

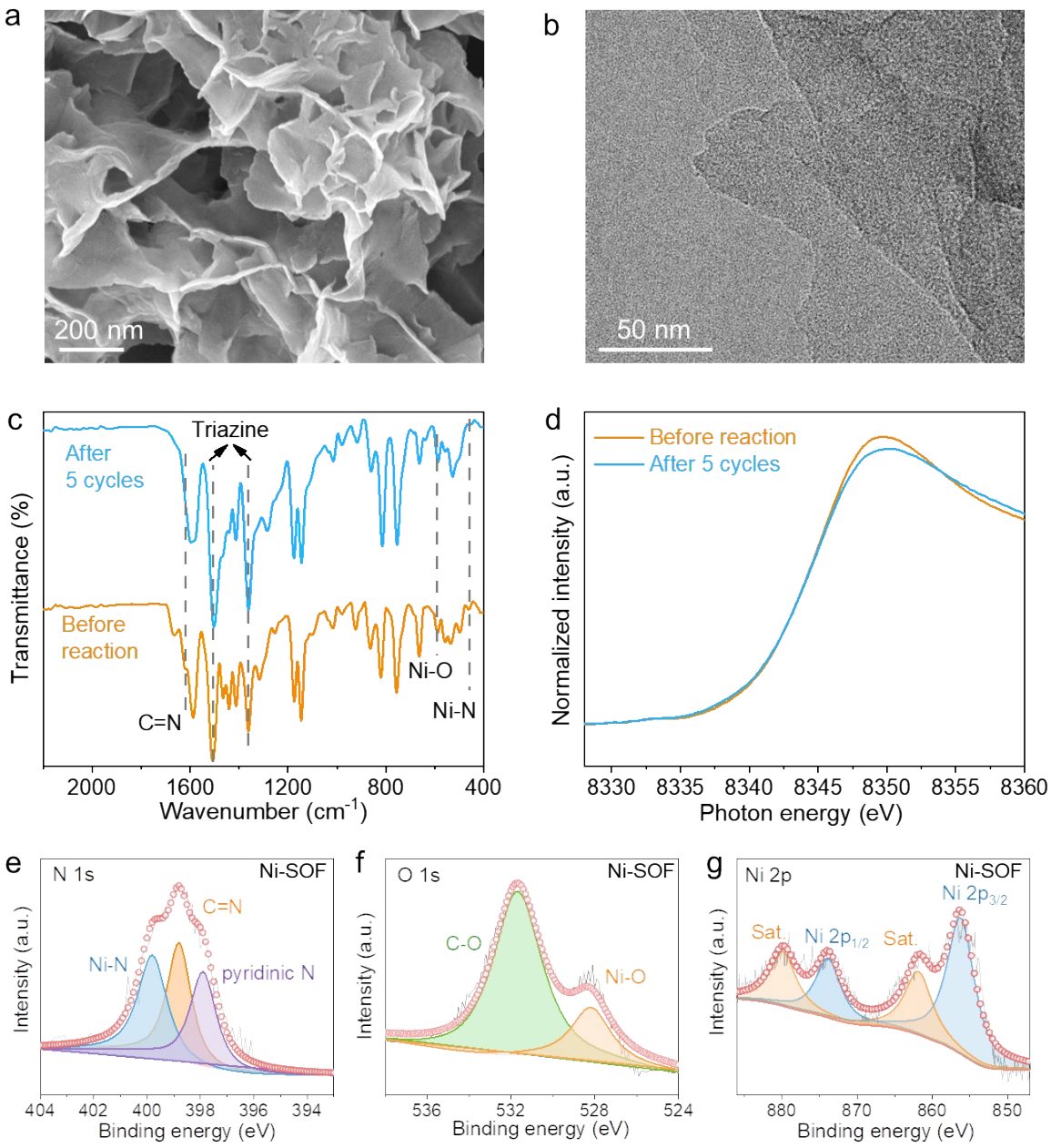

Fig. S15 (a) SEM and (b) TEM images of Ni-SOF after the cycling test. (c) FT-IR and (d) Ni K-edge XANES spectra of Ni-SOF before and after the cycling test. (e) N 1s, (f) O 1s, and (g) Ni 2p XPS spectra of Ni-SOF after the cycling tests.

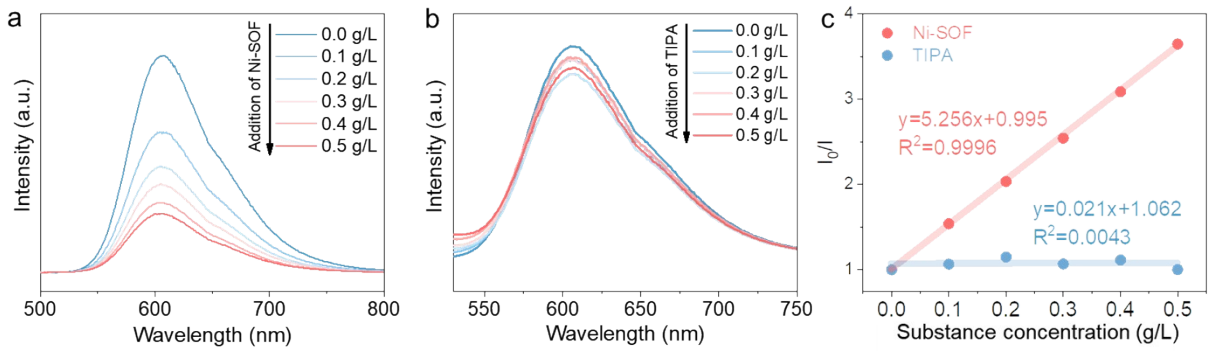

Fig. S16 (a,b) PL intensity of $[Ru(bpy)_3]Cl_2$ (1.6 mM) in the mixed solution of CH_3CN/H_2O (v:v = 3:1) with the addition of different amounts of (a) Ni-SOF and (b) TIPA at the excitation wavelength of 450 nm. (c) Corresponding Stern-Volmer plots (I_0 represents the initial emission intensity of the photosensitizer in solution and I represents the emission intensity of the photosensitizer in the presence of the catalyst or TIPA).

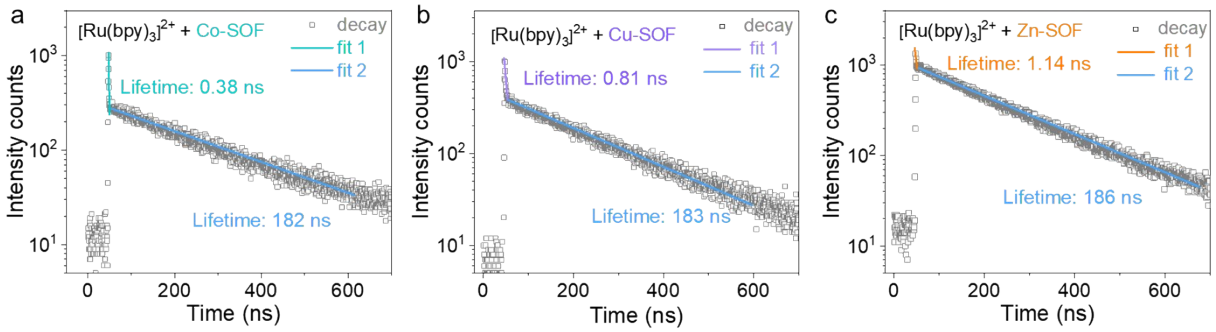

Fig. S17. Time-resolved PL spectra of $[Ru(bpy)_3]Cl_2$ in the presence of (a) Co-SOF, (b) Cu-SOF and (c) Zn-SOF.

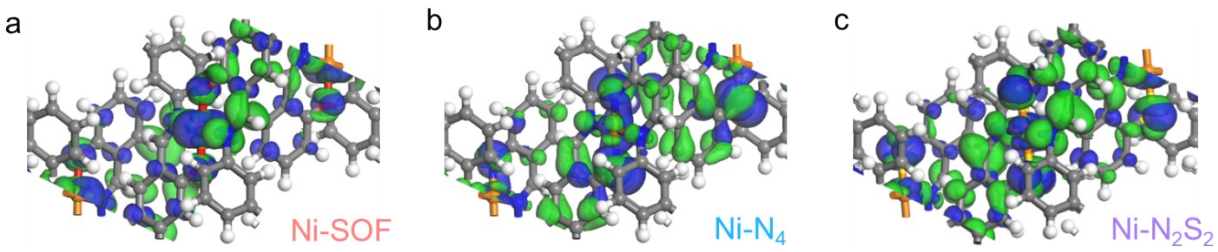

Fig. S18 3D contour plots of the electronic distributions near the Fermi level of (a) Ni-SOF, (b) $Ni-N_4$, and (c) $Ni-N_2S_2$. Orange balls represent Ni atoms, blue balls represent N atoms, red balls represent O atoms, yellow balls represent S atoms, grey balls represent C atoms, blue isosurfaces represent bonding orbitals, and green isosurfaces represent anti-bonding orbitals.

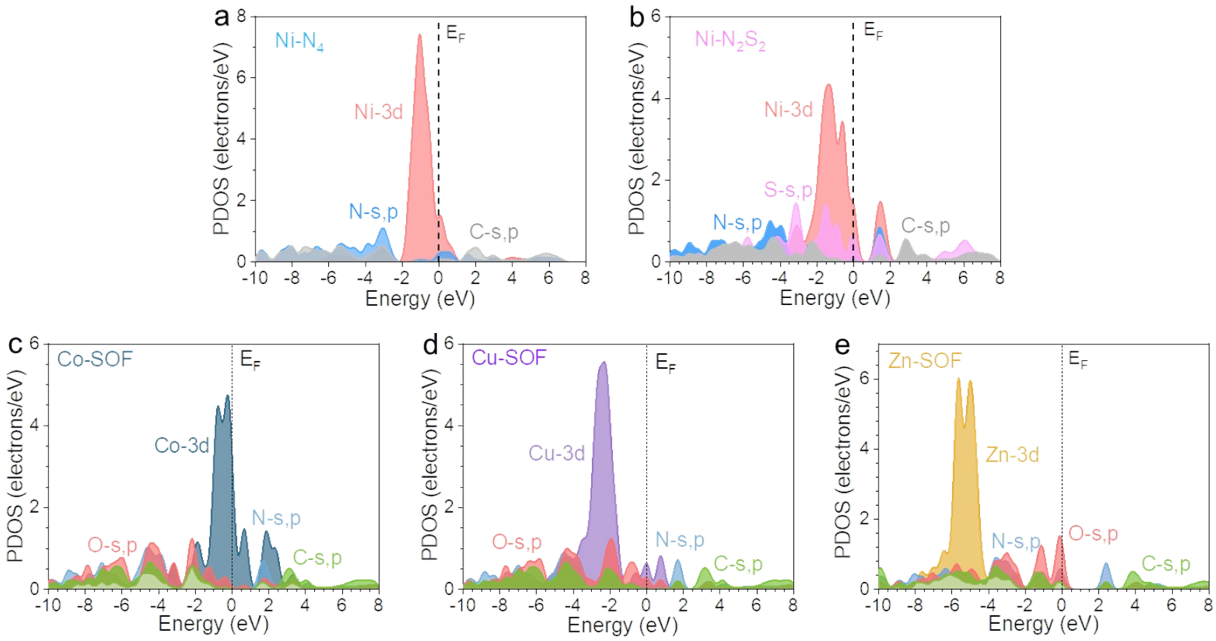

Fig. S19 PDOS spectra of (a) Ni-N_4, (b) Ni-N_2S_2, (c) Co-SOF, (d) Cu-SOF and (e) Zn-SOF.

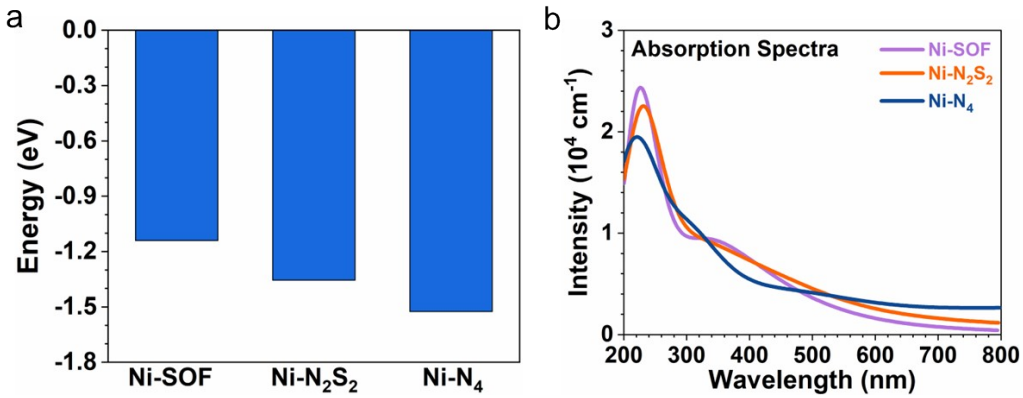

Fig. S20 The (a) d-band center and (b) optical property comparisons of different photocatalysts.

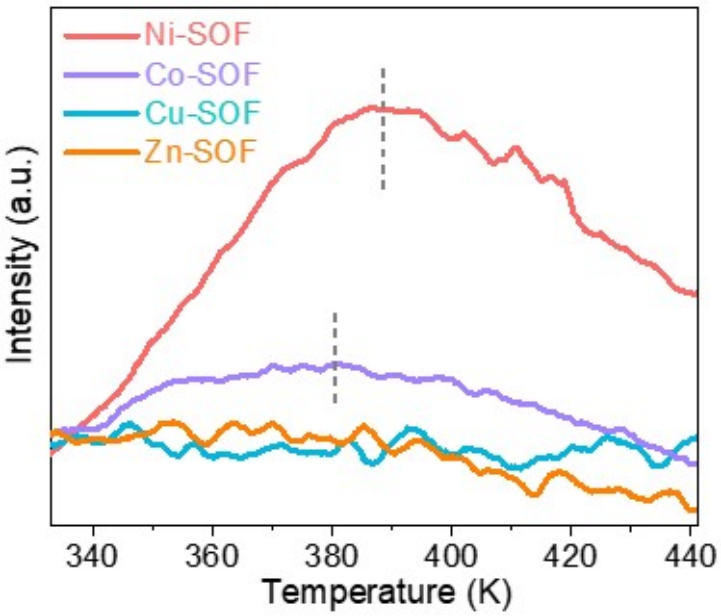

Fig. S21 CO_2 TPD spectra of Ni-SOF, Co-SOF, Cu-SOF, and Zn-SOF.

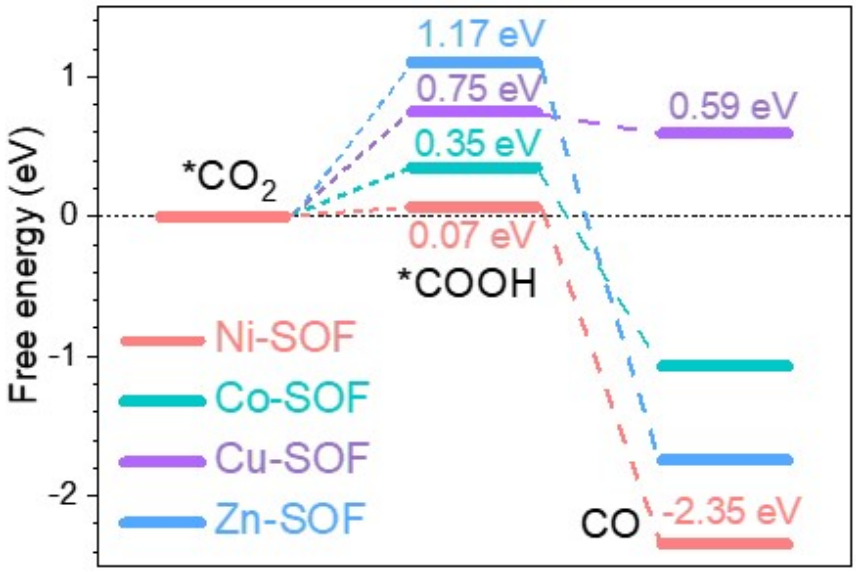

Fig. S22 Calculated free energy of CO_2 photoreduction on M-SOFs with different metal centers.

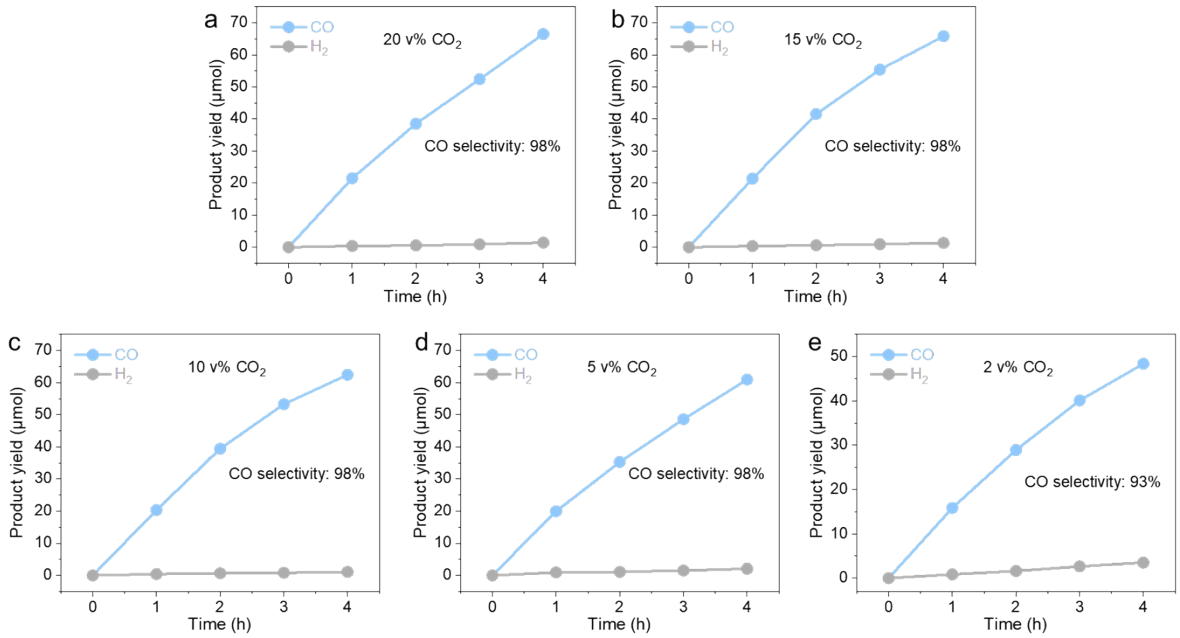

Fig. S23 Time-dependent CO and H_2 evolution on Ni-SOF under (a) 20 v%, (b) 15 v%, (c) 10 v%, (d) 5 v% and (e) 2 v% CO_2/Ar.

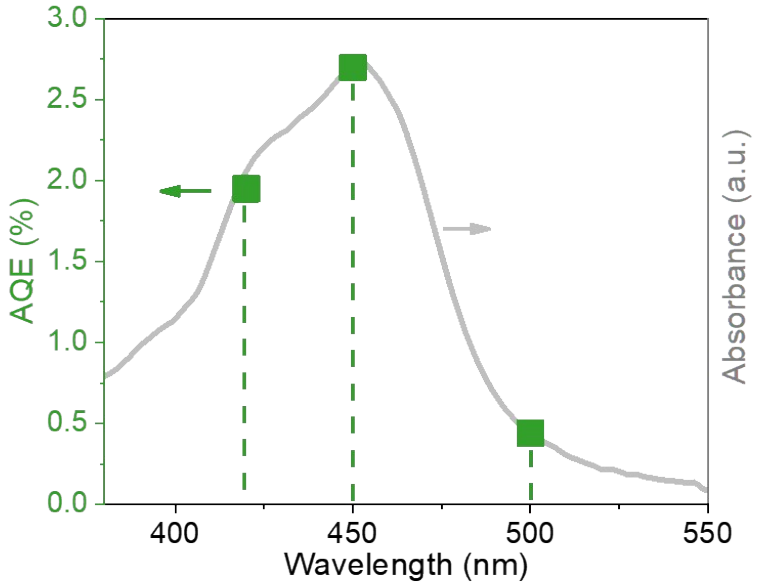

Fig. S24 AQE values of Ni-SOF at several selected wavelengths under 10 v% CO_2 overlapped with the absorption spectrum of $Ru(bpy)_3Cl_2$.

Table S1. Crystal data and structure refinement of Ni-salophen.

Identification code	**Ni-salophen**
Empirical formula	$C_{13}H_{10}NNi_{0.5}O$
Formula weight	225.57
Temperature/K	293
Crystal system	monoclinic
Space group	$P2_1/n$
a/Å	11.8362(4)
b/Å	7.6498(2)
c/Å	12.6345(4)
α/°	90
β/°	112.321(4)
γ/°	90
Volume/Å^3	1058.27(6)
Z	4
ρ_{calc}g/cm^3	1.416
μ/mm^{-1}	1.524
F(000)	468
Crystal size/mm^3	0.06 × 0.05 × 0.04
Radiation	CuKα (λ = 1.54184)
2Θ range for data collection/°	8.72 to 136.276
Index ranges	-10 ≤ h ≤ 14, -9 ≤ k ≤ 8, -15 ≤ l ≤ 12
Reflections collected	8659
Independent reflections	1918 [R_{int} = 0.0462, R_{sigma} = 0.0341]
Data/restraints/parameters	1918/0/142
Goodness-of-fit on F^2	1.091
Final R indexes [I>=2σ (I)]	R_1 = 0.0386, wR_2 = 0.1148
Final R indexes [all data]	R_1 = 0.0407, wR_2 = 0.1173
Largest diff. peak/hole / e Å^{-3}	0.33/-0.53

Table S2. Metal contents in M-SOFs measured by ICP.

M-SOF	Metal content (wt%)
Ni-SOF	10.5
Co-SOF	10.2
Cu-SOF	10.5
Zn-SOF	10.7

Table S3. Performance comparison of Ni-SOF with representative photocatalysts from literatures under pure CO_2.

Catalyst	Condition	CO activity ($\mu mol\ h^{-1}\ g^{-1}$)	CO selectivity	AQE	Ref.
Ni-SOF	**300 W Xe, λ≥420 nm MeCN/H_2O(3:1), Ru[a], TIPA[b]**	**16908**	**98%**	**2.8%**	**This work**
$Ni(OH)_2$-10%GR	300 W Xe, λ≥420 nm MeCN/H_2O (3:2), Ru, TEOA[c]	10725	96%	1.03%	*Nat. Commun.* **2020**, *11*, 5181.
2D-Ni_2TCPE	300 W Xe, 400-800 nm MeCN/H_2O (3:1), Ru, TEOA	2000	97%	--	*Angew. Chem. Int. Ed.* **2020**, *59*, 23588.
Ni-TpBpy	300 W Xe, λ≥420 nm MeCN/H_2O (3:1), Ru, TEOA	966	96%	0.3%	*J. Am. Chem. Soc.* **2019**, *141*, 7615.
COF-367-Co NSs	300 W Xe, λ≥420 nm 0.1 M $KHCO_3$, Ru, AA[d]	10162	78%	--	*J. Am. Chem. Soc.* **2019**, *141*, 17431.
m-NiAl-LDH	300 W Xe, 400-800 nm MeCN/H_2O (3:1), Ru, TEOA	712	70%	0.95% (CO + CH_4)	*Angew. Chem. Int. Ed.* **2019**, *131*, 11986.
BIF-29	300 W Xe, λ≥420 nm MeCN/H_2O (4:1), Ru, TEOA	3334	83%	0.078%	*Angew. Chem. Int. Ed.* **2019**, *58*, 11752.
Co-MOL@GO	5 W LED, λ=450 nm MeCN/H_2O (4:1), Ru(Phen)[e], TEOA	18008	95%	--	*Nat. Commun.* **2021**, *12*, 813.
MOF-Ni	300 W Xe, 420-800 nm MeCN/H_2O (13:1), Ru, TIPA	317	97%	--	*ACS Catal.* **2019**, *9*, 1726.
MOF-Co		1140	47%	--	
Ni@TPHH-COF	300 W Xe, λ=420 nm MeCN/H_2O (4:1), Ru, TEOA	1270	99%	--	*Adv. Funct. Mater.* **2021**, *32*, 2110136.
Ni-MOLs	5 W LED, 400-800 nm MeCN/H_2O (3:2), Ru, TEOA	12500	98%	2.2%	*Angew. Chem. Int. Ed.* **2018**, *57*, 16811.
$NiCo_2O_4$ HCs	5 W LED, 400-800 nm MeCN/H_2O (3:2), Ru, TEOA	10500	93%	1.86%	*Appl. Catal. B.* **2020**, *260,* 118208.
Ni-MOF	5 W LED, 400-800 nm MeCN/H_2O (3:2), Ru, TEOA	13600	97%	2.4%	*Appl. Catal. B.* **2021**, *283,* 119594.
LG/Nico-Co	300 W Xe, λ≥420 nm MeCN/H_2O (3:1), Ru, TEOA	13902	46%	--	*Angew. Chem. Int. Ed.* **2022**, *61*, e202205585.
Co_3O_4 platelets	300 W Xe, λ≥420 nm MeCN/H_2O (3:1), Ru, TEOA	3523	77%	0.069%	*Adv. Mater.* **2016**, *28*, 6485.
Co_3O_4-NS	5 W LED, 400-1000 nm MeCN/H_2O (3:2), Ru, TEOA	9040	70%	0.71%	*Appl. Catal. B.* **2019**, *244*, 996.
Cu_2S@ROH-$NiCo_2O_3$	300 W Xe, λ≥400 nm MeCN/H_2O (4:1), Ru, TEOA	7100	71.6%	--	*Angew. Chem. Int. Ed.* **2022**, *61*, e202205839.

a) Ru: $Ru(bpy)_3Cl_2$; b) TIPA: triisopropanolamine; c) TEOA: triethanolamine; d) AA: ascorbic acid; e) Ru(phen): $Ru(phen)_3(PF_6)_3$

Table S4. Performance comparison of Ni-SOF with representative photocatalysts from literatures under 10 v% CO_2.

Catalyst	Conditions	CO activity ($\mu mol\ h^{-1}\ g^{-1}$)	CO selectivity	Ref.
Ni-SOF	**300 W Xe, λ≥420 nm MeCN/H_2O (3:1), Ru[a], TIPA[b]**	**15610**	**98%**	**This work**
$Ni(OH)_2$-10%GR	300 W Xe, λ≥420 nm MeCN/H_2O (3:2), Ru, TEOA[c]	7432	92%	*Nat. Commun.* **2020**, *11*, 5181.
Ni-TpBpy	300 W Xe, λ≥420 nm MeCN/H_2O (3:1), Ru, TEOA	288.8	76%	*J. Am. Chem. Soc.* **2019**, *141*, 7615.
COF-367-Co NSs	300 W Xe, λ≥420 nm 0.1 M $KHCO_3$, Ru, AA[d]	2587	72%	*J. Am. Chem. Soc.* **2019**, *141*, 17431.
Ni@TPHH-COF	300 W Xe, λ=420 nm MeCN/H_2O (4:1), Ru, TEOA	3280	95%	*Adv. Funct. Mater.* **2021**, *32*, 2110136.
Ni-MOLs	5 W LED, 400-800 nm MeCN/H_2O (3:2), Ru, TEOA	11000	97%	*Angew. Chem. Int. Ed.* **2018**, *57*, 16811.
$NiCo_2O_4$ HCs	5 W LED, 400-800 nm MeCN/H_2O (3:2), Ru, TEOA	8900	89%	*Appl. Catal. B.* **2020**, *260,* 118208.
Ni-MOF	5 W LED, 400-800 nm MeCN/H_2O (3:2), Ru, TEOA	11900	97%	*Appl. Catal. B.* **2021**, *283,* 119594.
r-NiO	5 W LED, 400-1000 nm MeCN/H_2O (3:2), Ru, TEOA	6280	83%	*Nano Res.* **2021**, *14,* 730.
n-NiO		3940	65%	
$Ni_2(OH)(PO_4)$ NTs	5 W LED, 400-800 nm MeCN/H_2O (3:2), Ru, TEOA	5500	90.5%	*Nano Res.* **2021**, *14,* 2558.
$Ni_3(PO_4)_2$ bulk		2500	68%	

a) Ru: $Ru(bpy)_3Cl_2$; b) TIPA: triisopropanolamine; c) TEOA: triethanolamine; d) AA: ascorbic acid